Article

Mesozoic-Cenozoic Exhumation History of the Bogda Range, Eastern Tianshan: Insights from Apatite Fission Track Thermochronology

Shida Song [1,2], Jiangang Li [1], Xiaoyan Liu [2,3], Yadong Wang [4,5], Wentian Liang [1] and Sihua Yuan [2,3,*]

[1] State Key Laboratory of Continental Dynamics, Northwest University, Xi'an 710069, China
[2] Institute of Disaster Prevention, College of Earth Sciences, Sanhe 065201, China
[3] Hebei Key Laboratory of Earthquake Dynamics, Sanhe 065201, China
[4] Northwest Institute of Eco-Environment and Resources, Chinese Academy of Sciences, Key Laboratory of Petroleum Resources, Lanzhou 730000, China
[5] CAS Center for Excellence in Tibetan Plateau Earth Sciences, Chinese Academy of Sciences (CAS), Beijing 100101, China
[*] Correspondence: yuansihua@126.com

Abstract: The Bogda Range (hereafter referred to as the Bogda) is located in the Eastern Tianshan. Interpreting its tectono-thermal history is critical to understanding the intra-continental evolution of the Tianshan. In this study, we report new apatite fission track data from the late Paleozoic–Mesozoic sedimentary rocks in the northern Bogda and the Late Paleozoic granites in the southern Bogda to investigate the exhumation history of the Bogda. Apatite fission track ages dominantly range from the Jurassic to earliest Cenozoic (~143–61 Ma), except for one siliciclastic sample from the Early Permian strata with an older age of ~251 Ma. Thermal history modeling, together with detrital apatite fission track age peaks, reveal that the Bogda underwent three episodes of cooling during the Late Triassic, the Late Cretaceous, and the Late Miocene. The Late Triassic rapid cooling may represent the initial building of the Bogda, which is probably related to the final closure of the Paleo-Asian Ocean. During the Late Cretaceous, the Bogda may have experienced a moderate exhumation, which was possibly triggered by the extensive tectonic extension in the central–eastern Asian regime during the Cretaceous. The Late Miocene rapid cooling may be a response to the rapid uplift of the whole Tianshan, due to the far-field effect of the continuous India–Eurasia collision since the beginning of the Cenozoic.

Keywords: apatite fission track; thermochronology; exhumation history; Bogda; Tianshan

1. Introduction

The Tianshan, located on the southern margin of the Central Asian Orogenic Belt (Figure 1a), is the longest intracontinental mountain belt on Earth (3000 km long; [1,2]). The mountain belt was initially formed through a series of accretional events during the Paleozoic–Mesozoic (e.g., [3–8]), and experienced significant exhumations during the Mesozoic–Cenozoic (e.g., [9–12]). Geographically, the Chinese Tianshan can be divided into the Eastern Tianshan and the Western Tianshan along ~88 °E (Figure 1b). The Bogda, located in northern Eastern Tianshan (Figure 1b), was away from the active plate boundary and has recorded polyphase tectono-thermal events since the Mesozoic (e.g., [13–18]). Therefore, it is an ideal site to investigate the intra-continental evolution.

A critical question on how the Bogda was constructed has been continuously debated. There are currently two viewpoints. Some previous low-temperature thermochronology studies have emphasized that the Cenozoic exhumation in Bogda were mainly controlled by far-field stresses related to the India–Eurasia collision [12–15]. However, several recent studies argued that the Eastern Tianshan may be a Mesozoic topography [18–21].

Meanwhile, numerous Mesozoic planation surfaces preserved along the Bogda-Harlik Mountains [22,23] do not support an intense Cenozoic exhumation, and rather favor a Mesozoic topography of the East Tianshan. Hence, the tectonic evolution of the Bogda is still unclear.

In this work, we carried out apatite fission track analysis and thermal modeling in the Bogda from pre-Cenozoic sedimentary rocks in the northern Bogda and Late Paleozoic granites in the southern Bogda. The aim of this study is to constrain the cooling time and reconstruct the Mesozoic–Cenozoic evolution history of the Bogda.

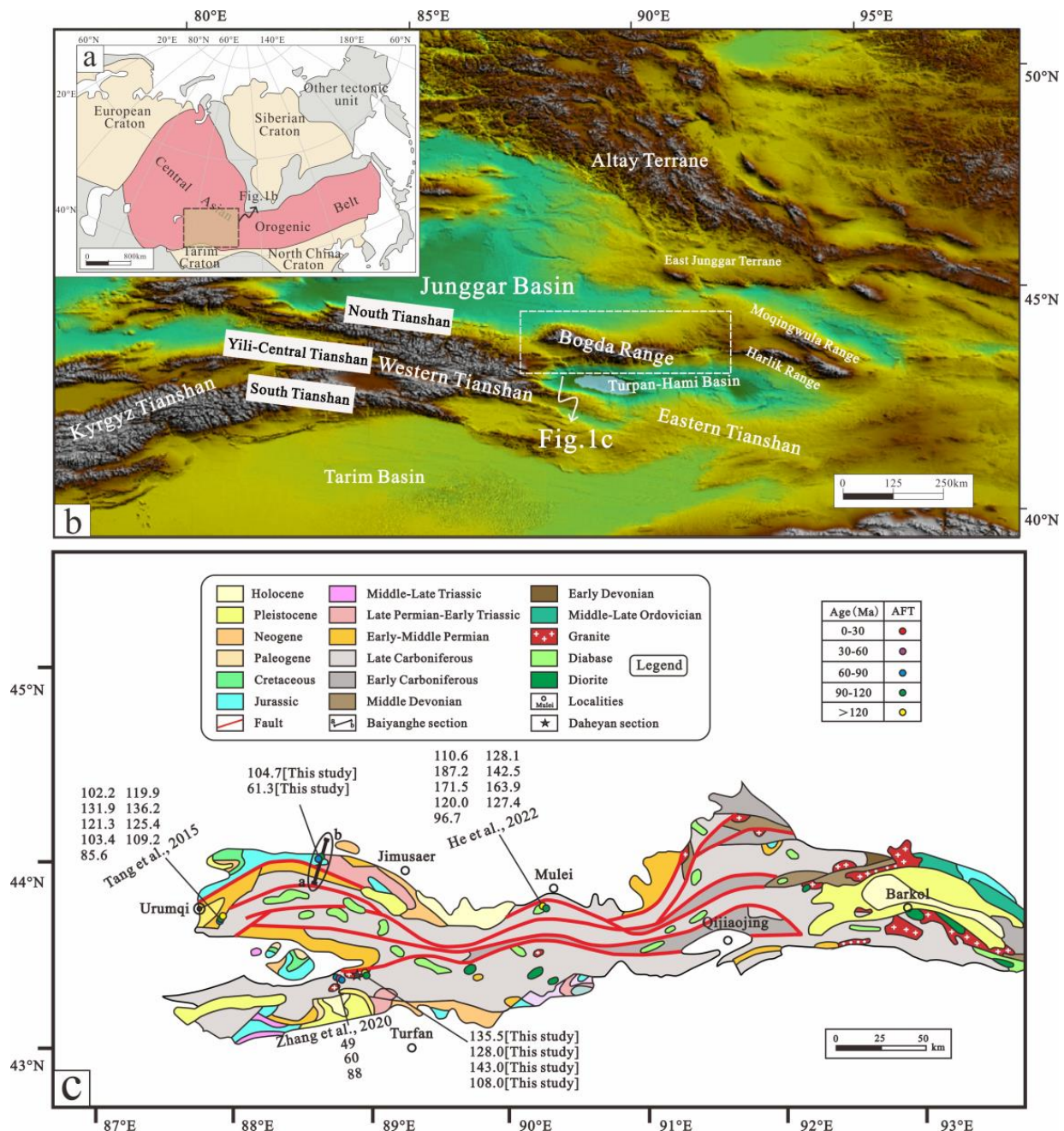
Figure 1. (**a**) Simplified tectonic map showing the position of the Central Asian Orogenic Belt (CAOB) and the Tianshan area (modified from [24]). (**b**) Topographic map of Chinese Tianshan-Junngar-Altai (modified from [25]). (**c**) Geological map of the Bogda, with Mesozoic apatite fission track ages (modified from [26]). The black star and a–b line are the sampling profile locations.

2. Geological Setting

The Bogda extends more than 400 km east–west from Urumqi to Qijiaojing and is a northward prominent arcuated mountain range. The northern margin of the Bogda is bounded by high-angle southward-dipping thrust faults, whereas the southern boundary of the Bogda is defined by northward-dipping thrust faults, also being the northern margin of the Turpan–Hami Basin. The main body of the Bogda is composed of Carboniferous submarine volcanic, pyroclastic, and carbonate rocks [3,27]. Permian-Cenozoic strata are exposed on both flanks of the range (Figure 1c; [25,28,29]). The Carboniferous strata can be divided into the Qijiaojing (C_1q), Liushugou (C_2l), and Qijiagou (C_2q) formations, which form a 1200–1800 m thick turbidite to the shallow marine sequence. Permian strata mainly consist of alluvial and lacustrine deposits. Triassic sedimentary rocks are mainly composed of mudstone, argillaceous siltstone, and sandy mudstone, indicating shallow lacustrine and braided river facies. The Jurassic depositional environments evolved from lacustrine and lake swamp settings in the Early–Middle Jurassic to an alluvial plain to a large alluvial fan setting in the Late Jurassic [30]. The Cretaceous strata are mainly exposed in the southern Junggar and northern Turpan-Hami basins. Cenozoic sedimentary rocks are characterized by terrestrial clastic deposits. The sedimentary rocks were collected from the Baiyanghe section, which is located in the transition zone between the Bogda and the Junggar Basin and mainly consists of Pre-Cenozoic sediments (Figure 1c).

No intense magmatism of post-Late Permian has been reported in the Bogda [16]. The Carboniferous mafic igneous rocks crop out along the Bogda. Granitoids are primarily distributed in the Daheyan region in the southern Bogda (Figure 1c), including granodiorite, monzonite, and diorite that formed during the Late Carboniferous [31,32].

3. Sampling and Analytical Methods

3.1. Sample Descriptions

Ten samples were collected for thermochronological dating and thermal history modeling along two sections in the Bogda (Table 1). Four samples of Carboniferous, Permian, Triassic, and Jurassic sedimentary rocks (BYH1, 2, 13, and 18) were collected from the Baiyanghe section in the northern Bogda (Figure 1c), and six Late Carboniferous granites (DHY1-6) were collected from the Daheyan section in the southern Bogda (Figure 1c; [31,32]).

Table 1. Geographic position and lithology details of the samples.

Sample	Lithology	Elevation (m)	Latitude (°N)	Longitude (°E)	Depositional or Crystallization Ages
BYH1	Pebbly sandstone	1725	43°57′44.80″	88°31′25.80″	Late Carboniferous
BYH2	Pebbly sandstone	1473	43°59′08.50″	88°31′36.50″	Early Permian
BYH13	Tuffaceous sandstone	1007	44°03′29.51″	88°31′29.55″	Late Jurassic
BYH18	Tuffaceous sandstone	975	44°04′58.20″	88°31′35.09″	Early Triassic
DHY1	Granite	1867	43°24′43.44″	88°51′53.94″	Late Carboniferous
DHY2	Granite	1881	43°24′46.13″	88°51′59.90″	Late Carboniferous
DHY3	Granite	1826	43°23′47.80″	88°51′16.50″	Late Carboniferous
DHY4	Granite	1850	43°23′43.44″	88°51′20.37″	Late Carboniferous
DHY5	Granite	1926	43°23′47.77″	88°51′31.96″	Late Carboniferous
DHY6	Granite	1889	43°24′11.43″	88°51′50.15″	Late Carboniferous

We selected two representative granite samples from the Daheyan section for petrological analysis (DHY6 and DHY1; Figure 2). DHY6 is pink and has a granitic texture and massive structure (Figure 2a). It consists of alkali feldspar (50%, including orthoclase and K-feldspar), plagioclase (25%), quartz (20%), clinopyroxene (3%), and minor accessory minerals (2%), including apatite and zoisite (Figure 2b). DHY1 is light red in color, and has subhedral crystals and a massive structure (Figure 2c), consisting of plagioclase (65%), amphibole (15%), quartz (15%), and biotite (5%), and is slightly altered (Figure 2d).
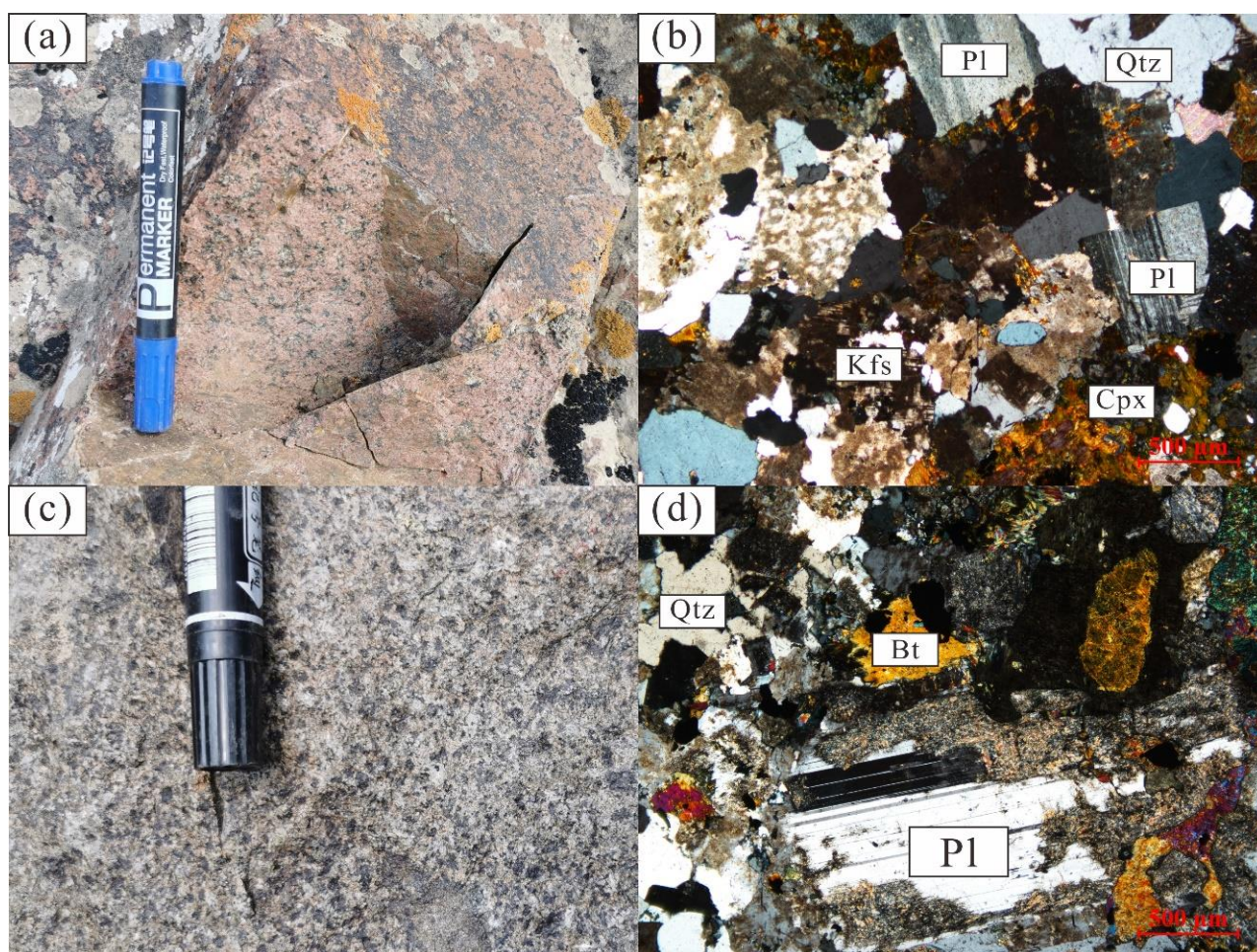
Figure 2. Field outcrops and microphotographs of representative samples from the Daheyan section. (**a**,**b**) DHY6; (**c**,**d**) DHY1. Qtz, quartz; Pl, plagioclase; Bt, biotite; Kfs, K-feldspar; Cpx, Clinopyroxene.

3.2. Analytical Methods

Apatite separation and fission track dating were performed at the Geochemical Analysis and Testing Center, Northwestern Institute of Eco-Environment and Resources, Chinese Academy of Sciences, Lanzhou, China. Apatite fission track ages were determined using the external detector method [33]. The apatite crystals were separated from rock samples by crushing, vibration, magnetic, and heavy liquid separation. The separated apatite grains were fixed onto glass slides using epoxy resin and then ground and polished to expose the maximum inner surface. The samples were then etched in 5.5 N HNO_3 for 20 s at 21 °C [34,35] to reveal spontaneous fission tracks. The sample mounts, age standards, and IRMM540R dosimeter samples were irradiated together in a thermal reactor at Oregon State University in America using the thermal neutron fluence around 1.0×10^{16} cm^{-2}. After irradiation, the external muscovite detectors were etched in 40% HF for 40 min at 20 °C to reveal induced fission tracks. The zeta (ζ) calibration method was calibrated based on calculating apatite fission-track ages [33,36]. A ζ value of 265.8 ± 7.98 a·cm^2 was obtained using the Durango and Fish Canyon apatite standards [33,37]. Fission tracks were counted on a Zeiss microscope using the Autoscan system (produced in Australia) in manual mode, set to a magnification of ×1000. Confined track length and D_{par} values were measured on digital images captured by a Zeiss camera. All central ages, to within an error of 1 σ, were determined by using the Radial Plotter program in [38].

4. Results and Thermal History

4.1. Apatite Fission Track Ages

Only seven samples yielded visible grains for apatite fission-track analysis, and the detailed data are listed in Table 2. The samples yield a wide range of apatite fission track central ages, which vary from 251.0 ± 26.0 to 61.3 ± 7.7 Ma. These are all younger than their stratigraphic or crystallization ages, except for some ages in sample BYH2 (Figure 3). All single-grain age distributions passed the χ^2 test [P(χ^2) $\geq$ 5%] except for sample BYH13, implying a broad single-grain age distribution for BYH13 and homogenous single-grain age distributions for the other samples [39]. The samples yielded D_{par} values of 1.83–3.02 μm. The measured confined track lengths were corrected for their crystallographic orientation using the HeFTy program (c axis-corrected fission track length, L_c; [34,40,41]). Four samples (BYH2, BYH13, DHY1, and DHY2) were found to yield sufficient measurable confined tracks. The mean track lengths yield of 12.69 ± 1.50 to 12.81 ± 1.24 μm. These are shorter than the track lengths found in rapidly cooled rocks (16.3 μm; [42]), suggesting long-term residence in the partial annealing zone (60–120 °C) or a complicated thermal history.

Table 2. Apatite fission-track data. ρs and ρi, spontaneous and induced track densities; ρd, dosimeter track densities; ^{238}U, concentration of ^{238}U; P(χ^2) (%), chi-square probability, P(χ^2) $\geq$ 5% indicate a homogenous population [39]; D_{par}, the mean length of fission-track etch pit; L, the mean track length with c-axis projection; and n, number of lengths measured. Ages were calculated using the Radial Plotter program in [38], using a zeta value of 265.8 ± 7.98.

Sample	Number of Grains	ρs($\times 10^5$cm^{-2}) (Ns)	ρi($\times 10^5$cm^{-2}) (Ni)	ρd($\times 10^5$cm^{-2}) (Nd)	^{238}U (ppm)	P(χ^2) (%)	Central Age ($\pm 1\sigma$) (Ma)	Dpar (μm)	L (μm $\pm 1\sigma$) (n)
BYH2	21	5.08 (290)	2.82 (161)	10.7 (17142)	3.78	100	251.0 ± 26.0	2.67	12.81 ± 1.24 (44)
BYH13	34	2.94 (421)	8.83 (1263)	12.2 (17142)	9.63	0	61.3 ± 7.7	2.18	
BYH18	36	8.64 (456)	12.50 (660)	11.5 (17192)	18.11	70	104.7 ± 7.1	3.02	12.75 ± 1.47 (43)
DHY1	32	9.69 (766)	10.24 (810)	10.8 (17142)	12.25	8	135.5 ± 8.8	2.13	12.82 ± 1.37 (68)
DHY2	19	7.72 (321)	10.30 (428)	12.5 (17192)	10.50	9	128.0 ± 12.0	2.10	12.69 ± 1.50 (100)
DHY4	19	4.22 (266)	4.47 (282)	11.5 (17142)	5.18	66	143.0 ± 13.0	2.13	
DHY6	21	5.01 (292)	6.73 (392)	11.0 (17192)	9.24	39	108.0 ± 9.0	1.83	11.90 ± 1.76 (7)

Sample BYH13 failed to pass the χ2 test, so we used Radial Plotter [38] to distinguish the different clusters of ages in the clastic samples (Figure 4). The decomposed sample ages yield three age peaks: P1 at 251 Ma, P2 at 104.7–99.2 Ma, and P3 at 24.9 Ma (Figure 4). Some single-grain ages in sample BYH2 are older than its stratigraphic age, which suggests that the sample was not fully annealed and its peak age has no geological significance. All of the single-grain ages from samples BYH13 and BYH18 are younger than their stratigraphic ages. Their peak ages are only used as a reference for the discussion, due to the limited apatite grains [43].

The granitic apatite fission-track ages are positively correlated with its altitude (Figure 5). Samples DHY4, DHY1, and DHY2 yield central ages of 143.0 ± 13.0 to 128.0 ± 12.0 Ma over elevations of 1850–1881 m. The young central age (108.0 ± 9.0 Ma) of the sample with the highest elevation (1889 m; DHY6) is similar to the age peak P2 (104.7–99.2 Ma) in the Baiyanghe section.
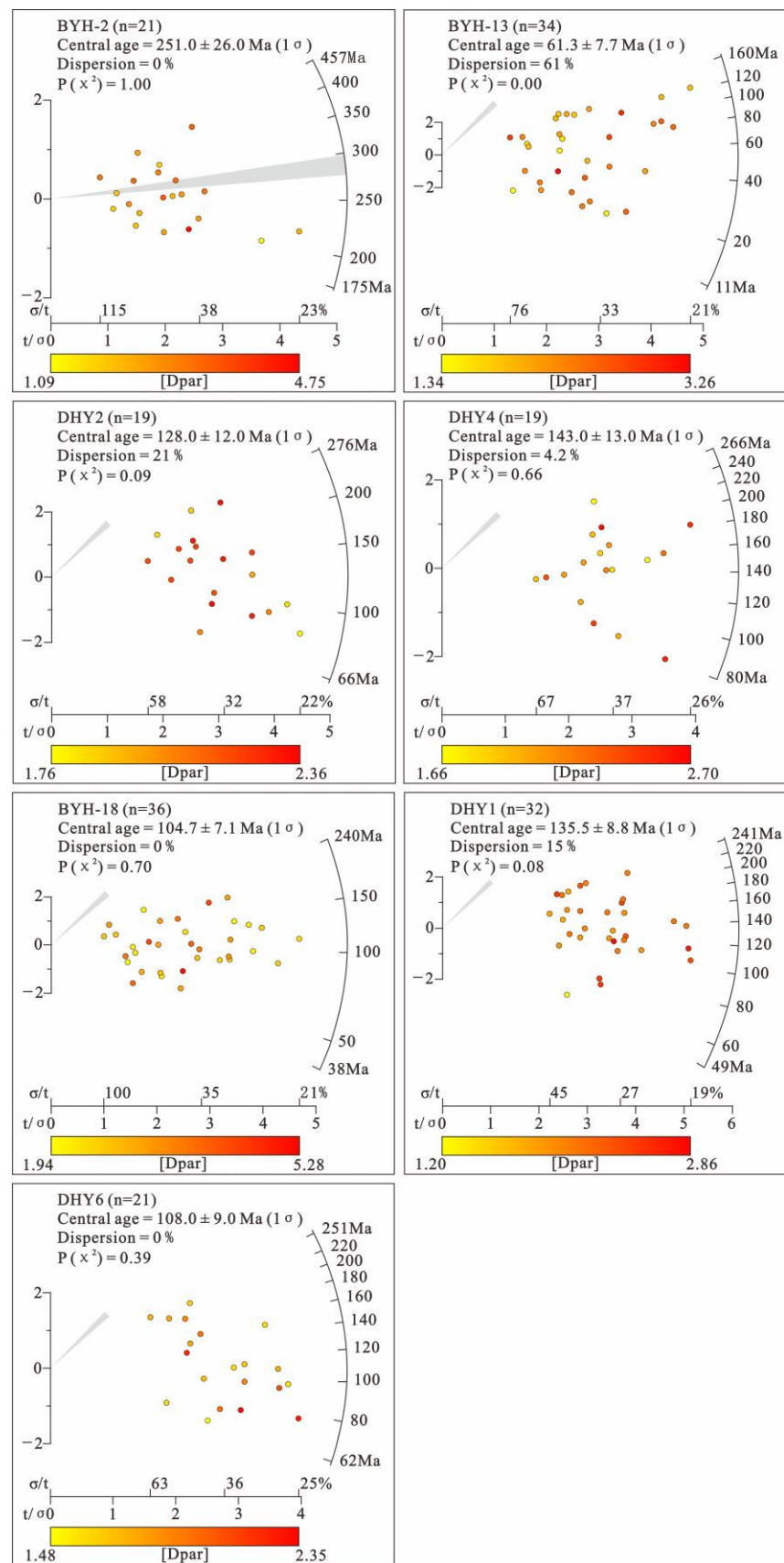
Figure 3. Radial plots for samples from the Bogda. Radial plots were constructed using the Radial Plotter program in [38]. The gray area corresponds to stratigraphic or crystallization age.
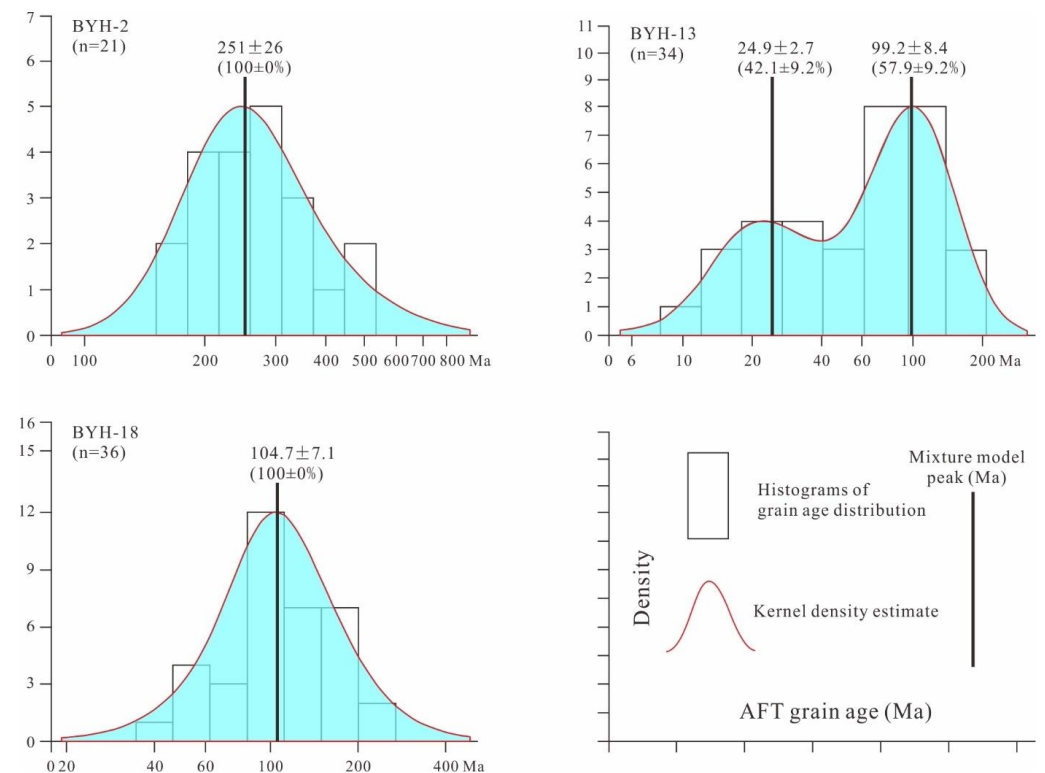
Figure 4. Density plot of apatite fission track ages. Density plots were constructed using the Radial Plotter program in [38].
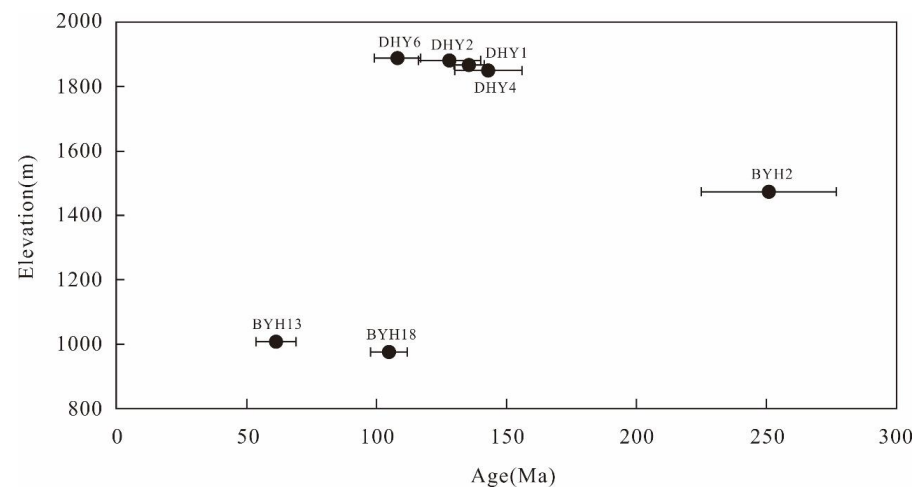

Figure 5. Apatite fission track age versus elevation.

4.2. Thermal History Modeling

The HeFTy program (version 1.9.3) was applied to calculate single cooling paths using a Monte Carlo algorithm [34,41,44], based on the annealing model of [41]. D_{par} was selected as the kinetic annealing parameter and the initial track length was assumed to be 16.3 μm. We performed the modeling for samples with sets of at least 50 track-length measurements, and, as often as possible, with sets of 100 measurements (Table 2; [45]). The simulation ended when 100,000 acceptable paths had been produced. The modeling results were evaluated by length and age goodness-of-fit (GOF) values: GOF values of >0.05 were considered to be acceptable and GOF values of ≥0.5 were considered as good [34]. For sample BYH-18, we set the start of the model to its stratigraphic age and assumed that the Mesozoic surface temperature of the Junggar Basin was about 15 ± 10 °C. For the

granitic modeling, we assumed that all samples have totally annealed at a sufficiently high temperature (160–200 °C) at a certain age (200–270 Ma) older than the apparent fission track age, following the modeling strategies suggested by [46,47]. A present-day mean surface temperature of 15 ± 10 °C was applied as another parametric condition.

The modeled T–t paths are shown in Figure 6. In our thermal history models, all granitic samples show rapid cooling in the Late Triassic, the Late Miocene, and relatively moderate cooling since the Late Cretaceous. Sample DHY1 cooled rapidly from ~120 °C to ~85 °C during ~230 ± 10 Ma, then stayed in the apatite partial-annealing zone (APAZ; 120–60 °C) for a long time (>100 Ma). Since ~100 Ma, the cooling rate of sample DHY1 began to increase and kept a slow to moderate rate until the rock cooled to near-surface conditions. Sample DHY2 has a similar cooling path to sample DHY1, except that the Late Cretaceous cooling acceleration began from ~75 Ma. After 10 Ma, both the cooling of both granitic samples rapidly crossed the upper APAZ isotherm. Sample BYH18 was buried and heated to full annealing at ~200–100 Ma, then cooled into the APAZ from ~50 Ma. After 10 Ma, the sample also cooled rapidly to the surface temperature.
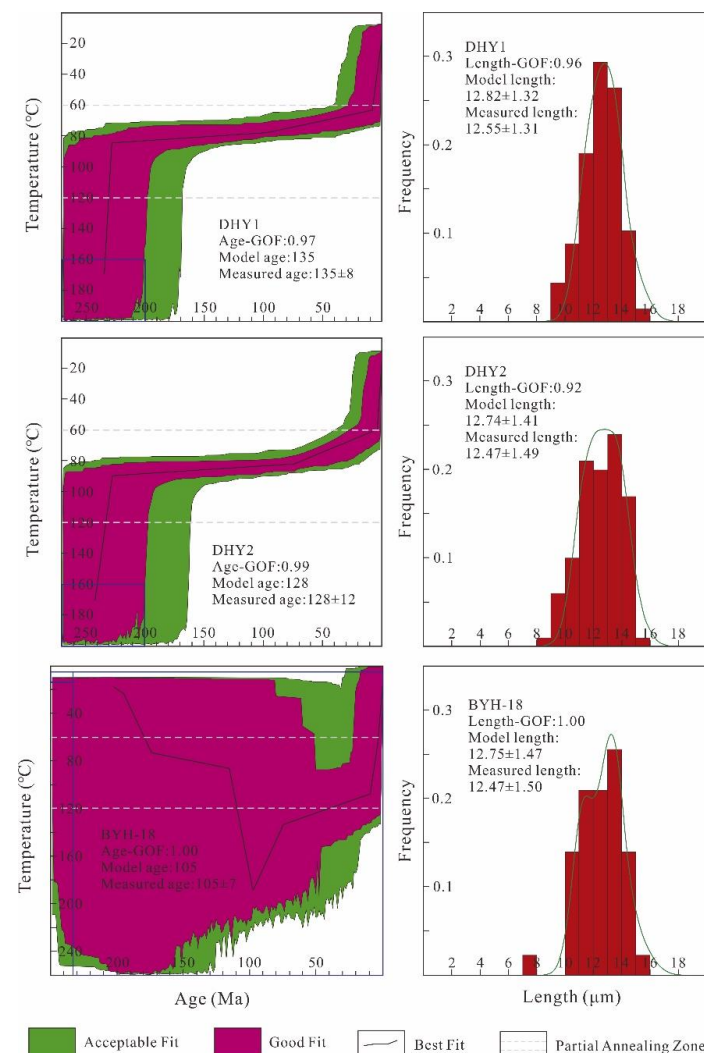

Figure 6. Modeled inverse time–temperature (t-T) paths and length distribution for DHY1, DHY2, and BYH18. GOF is the goodness of fit between the data measured and those predicted by the model. Cooling paths of individual samples were calculated with HeFTy [34,47], based on the annealing model of [41]; blue box is the constraint box.

5. Interpretations and Discussion

A total of six samples were valid, with single-grain ages less than their stratigraphic or crystallographic ages, including two pre-Cenozoic clastic samples collected from the Baiyanghe section in the northern Bogda and four Late Carboniferous granite samples collected from the Daheyan area in the southern Bogda (Figure 1c). The obtained results mainly show the apparent apatite fission-track ages from Jurassic to earliest Cenozoic (Table 2). Hence, on both sides of the Bogda, a clear Mesozoic low-temperature geochronology signal has been preserved (Figure 1c; [16–18]). Nevertheless, the single-grain ages of our samples display a certain degree of dispersion (Figure 3). As mentioned earlier, four Late Carboniferous granitic samples (DHY1, 2, 4, and 6) are collected along a vertical profile with a small elevation difference (<~200 m; Table 1). Therefore, we inversed the thermal history of three samples. The age distribution of clastic samples was used as a reference to further constrain the evolution of the Bogda. Our results, combined with geological and thermochronological evidence, reveal that the Bogda experienced three exhumation episodes, rapid exhumation during the Late Triassic and the Late Miocene, and moderate exhumation during the Late Cretaceous (Figures 4 and 6).

5.1. Late Triassic

According to our thermal history modeling results from the Late Carboniferous granites in the southern Bogda, all samples show a rapid cooling phase during the Late Triassic. Both sample DHY1 and sample DHY2 cooled from ~120–85 °C at ~230 ± 10 Ma (Figure 6). This result is consistent with the Triassic–Jurassic cooling recorded by thermal history models of Late Carboniferous volcanic rocks near Mulei county in the northern Bogda [18]. Additionally, many pieces of geological, seismic, and sedimentary evidence suggest that the Bogda experienced a rapid uplift during the Late Triassic [48–52]. For example, some scholars observed that the folded Upper Triassic are unconformably overlain by the Lower Jurassic in the northern Bogda (Jimusaer area) [48,51]. In the southern Bogda (Chaiwopu depression), the seismic profile also reveals characterized sedimentary discontinuity and unconformity [52]. The Upper Triassic Xiaoquangou Group are mainly coarse clastic deposits, indicating a paleocurrent direction from the ridge toward both flanks of the mountain, which was distinguished from the direction recognized from the Kelamayi Formation of the Middle Triassic [48–50]. These pieces of evidence are consistent with our results, all indicating a rapid exhumation and geomorphic process of the Bogda during the Late Triassic.

With regard to the whole Tianshan, Triassic cooling signals (through low-temperature thermochronology) have been preserved in many areas. In Eastern Tianshan, detrital apatite fission-track data from the Moqingwula Range record the main peak age of 222 Ma, which is indicative of rapid Late Triassic cooling in the mountain hinterland [21]; in the Yandong copper deposit, a rapid Late Triassic (~230–210 Ma) cooling has been identified from apatite fission-track thermal history models of the basement [53]; based on fission-track thermochronology, detrital apatite from the Jurassic and Early Cretaceous sandstones in the East Junggar show significant Middle–Late Triassic cooling ages of ~237–228 Ma [19]. Additionally, several Late Triassic–Middle Jurassic apatite fission track ages have been reported in the Western Tianshan and foreign Tianshan, such as the low-relief sections of the Tianshan (e.g., the Kyzylkum-Nurata section in Uzbekistan and Junggar-Aratau Mountains in Kazakhstan; [54,55]), the uplifted plateau basins (e.g., the Song-Kul Basin and Issyk-Kul Lake in Kyrgyzstan; [56,57]), and large regional strike–slip faults (e.g., the Talas-Fergana fault and Nalati fault; [58,59]). Late Triassic–Early Jurassic conglomerate deposits are observed in both the Junggar and Tarim basins, also suggesting the Late Triassic exhumation in the Tianshan and the subsequent rapid accumulation of basin sediments [60–63].

Corresponding to the Triassic exhumation, a ~240–235 Ma dextral shear motion has been observed in the Xingxingxia shear zone [64]. The mylonitized schist in the Yamansu shear zone exhibits a ~212 Ma sericite ^{40}Ar/^{39}Ar age [65]. The thermochronological signals,

combined with fault activities, may suggest intense Late Triassic tectonic activity across the Tianshan. Previous studies attributed this event to the collision between the Qiangtang Block and southern Eurasia since the Middle Triassic (e.g., [19,56,58,66,67]). However, a growing body of research considers that the Triassic cooling signals in Tianshan may be a response to the final closure of the Paleo-Asian Ocean (e.g., [8,20,68]). Therefore, the Late Triassic rapid exhumation may imply the initial building of the Bogda.

5.2. Late Cretaceous

The thermal history inversion results of two granite samples in the southern Bogda, both of which show a lower cooling rate since the Late Triassic, until the Late Cretaceous when the cooling rates began to increase with a slow growth rate (Figure 6), possibly indicating a Late Cretaceous moderate exhumation of the Bogda. As for the detrital samples from the northern Bogda, the single-grain ages of the early Triassic sandstone (sample BYH18) and the Late Jurassic sandstone (sample BYH13) were both younger than their depositional ages (Figure 3), suggesting that the samples may be deposited and buried to a depth below the APAZ. According to geological investigation results [48,69], the thickness of Triassic to Cretaceous strata in the southern Junggar is over 5 km, forming sufficient burial conditions that could reset or at least partly reset the apatite fission track system. Therefore, the age peaks of the detrital samples possibly represent post-resetting events. Samples BYH13 and BYH18 both exhibit major age peaks at 104.7–99.2 Ma, and may also imply the Late Cretaceous exhumation of the Bogda (Figure 4).

Based on apatite fission-track data and a synthesis of the previous literature, He et al. [19] identified clear slow to moderate regional exhumation throughout the Eastern Tianshan during the Cretaceous, which supports the Late Cretaceous exhumation constrained by our results. In the Bogda, a Cretaceous exhumation (~110 Ma) has been reported from the apatite fission-track thermochronological data of basement and detrital samples [18]. In the northern Barkol Basin, Chen et al. [21] defined a rapid cooling in the Moqingwula Range from 113–92 Ma, based on the distribution of the detrital apatite fission-track ages. Near this region, the Late Cretaceous cooling was also documented by apatite fission-track thermal history modeling of the basement in the Harlik Mountains [20]. During the Cretaceous, central-eastern Asia represents one of the largest crustal extensional provinces worldwide, marked by various extensional tectonics including metamorphic core complexes, (half) graben basins, and basaltic, granitic, and minor ultramafic intraplate magmatism ([70,71], and references therein). This tectonic extension event could be product of the mantle plume upwelling triggered by the Perm Anomaly on the core–mantle boundary during the mid-Cretaceous [70]. The moderate exhumation of the Eastern Tianshan during the Late Cretaceous may a reflex to the tectonic extension event that occurred in central-eastern Asia during the Cretaceous.

According to the summary of published detrital zircon U-Pb data and sedimentary analyses, Fang et al. [72] suggested that North Tianshan continued to uplift and served as a main source terrane for the sediments (Donggou formation) in the southern Junggar Basin during the Late Cretaceous. We consider that the Bogda may have experienced moderate exhumation since the Late Cretaceous, which may have led to the building of the Mesozoic low-relief surfaces preserved along the Bogda-Harlik Mountains [22,23].

5.3. Late Miocene

The thermal history models for samples from the Bogda (BYH18, DHY1, and DHY2) reveal evidence for rapid exhumation during the Late Miocene (10 Ma) (Figure 6). This rapid cooling was also recorded in other areas of the Bogda by apatite fission-track data [13,14,73]. Using the same method, Zhang et al. [74] and Zhu et al. [75] confirmed rapid cooling in the North Tianshan and Jueluotage Range at ca. 10 Ma. Zircon U-Pb chronology and heavy mineral analysis in the Kuitunhe area also reveal an episode of tectonic uplift in the North Tianshan at ca. 7 Ma [76]. The rapid uplift of the North Tianshan during the late Miocene (ca. 7 Ma) is also supported by magnetostratigraphic and magnetic susceptibility anisotropy

data from the southern Junggar Basin [77,78]. Using the timing of the deposition of the earliest syn-tectonic growth strata, Sun et al. [79] suggested that a sharp orogeny began in the Middle Tianshan at ca. 6 Ma. The (U-Th)/He ages from the Kekesu area also suggest a rapid denudation event in the Middle Tianshan at ca. 5 Ma [80]. Cenozoic deformations in the thrust fold belt in the northern Kuqa Depression identified in two-dimensional seismic reflection profiles imply that the rate of shortening increased at ca. 5.5 Ma in the South Tianshan [81]. This is consistent with (U-Th)/He and apatite fission-track data from the South Tianshan [82,83]. In addition, thermochronological data and sedimentary records in northern Tibet and the surrounding areas provide regional evidence for a rapid orogeny beginning in the late Miocene [84].

The rapid uplift and exhumation of the Tianshan since the Late Miocene (ca. 10 Ma) is supported by a wide range of data from thermochronological, geodesic, sedimentological, and magneto-stratigraphical studies (e.g., [66,85,86]), and this uplift probably spread to the Tianshan foreland. Conglomerate clast and detrital zircon U-Pb data from Cenozoic sedimentary rocks in the southern Junggar Basin suggest that the uplift during the middle–late Miocene (12–7 Ma) most likely occurred in the hinterland and foreland of the entire Tianshan [87]. A study of the syn-tectonic growth strata, magneto-stratigraphy, and low-temperature thermochronology in the Kuqa Depression showed that the Cenozoic deformation and uplift of the Tianshan became more pronounced in the Late Miocene (13–10 Ma) and extended to the entirety of the Tianshan and the basin–orogen boundary [1]. It is generally thought that the continuous India–Eurasia collision may be the main driving force (e.g., [62,78,87–89]).

6. Conclusions

Our new apatite fission-track data combined with thermal history inverse modeling suggest two exhumation events in the Bogda: rapid exhumation in the Late Triassic and the Late Miocene, and moderate exhumation in the Late Cretaceous. The first event was mainly identified by the thermal history inverse modeling of the granites in the southern Bogda; all samples show a rapid cooling phase during the ~230 ± 10 Ma. It may represent the initial building of the Bogda, which is related to the final closure of the Paleo-Asian Ocean. The second event was shown in the granitic thermal history models as an increase in the cooling rate in the Late Cretaceous (~100 or ~75 Ma), and exhibit main age peaks at 104.7–99.2 Ma in the detrital samples. The relatively low cooling rate possibly implied a moderate exhumation of the Bogda in the Late Cretaceous, which may have been triggered by the tectonic extension that occurred in central-eastern Asia during the Cretaceous. The last event was identified by all thermal history inverse modeling. The Late Miocene cooling signals were distributed in the whole Tianshan and the continuous India–Eurasia collision may have been its main driving force.

References

1. Windley, B.F.; Alexeiev, D.; Xiao, W.; Kroner, A.; Badarch, G. Tectonic models for accretion of the Central Asian Orogenic Belt. *J. Geol. Soc.* **2007**, *164*, 31–47. [CrossRef]
2. Xiao, W.J.; Huang, B.C.; Han, C.M.; Sun, S.; Li, J.L. A review of the western part of the Altaids: A key to understanding the architecture of accretionary orogens. *Gondwana Res.* **2010**, *18*, 253–273. [CrossRef]
3. Allen, M.B.; Windley, B.F.; Zhang, C. Palaeozoic collisional tectonics and magmatism of the Chinese Tien Shan, central Asia. *Tectonophysics* **1993**, *220*, 89–115. [CrossRef]
4. Gao, J.; Li, M.; Xiao, X.; Tang, Y.; He, G. Paleozoic tectonic evolution of the Tianshan Orogen, northwestern China. *Tectonophysics* **1998**, *287*, 213–231. [CrossRef]
5. Charvet, J.; Shu, L.; Laurent-Charvet, S. Paleozoic structural and geodynamic evolution of eastern Tianshan (NW China): Welding of the Tarim and Junggar plates. *Epis. J. Int. Geosci. Seoul Natl. Univ.* **2007**, *30*, 162–186.
6. Charvet, J.; Shu, L.; Laurent-Charvet, S.; Wang, B.; Faure, M.; Cluzel, D.; Chen, Y.; De Jong, K. Palaeozoic tectonic evolution of the Tianshan belt, NW China. *Sci. China Earth Sci.* **2011**, *54*, 166–184. [CrossRef]
7. Xiao, W.J.; Windley, B.F.; Allen, M.B.; Han, C.M. Paleozoic multiple accretionary and collisional tectonics of the Chinese Tianshan orogenic collage. *Gondwana Res.* **2013**, *23*, 1316–1341. [CrossRef]
8. Tan, Z.; Xiao, W.J.; Mao, Q.G.; Wang, H.; Sang, M.; Li, R.; Gao, L.M.; Guo, Y.H.; Gan, J.M.; Liu, Y.H.; et al. Final closure of the Paleo Asian Ocean basin in the early Triassic. *Commun. Earth Environ.* **2022**, *3*, 259. [CrossRef]
9. Hendrix, M.S.; Dumitru, T.A.; Graham, S.A. Late Oligocene-early Miocene unroofing in the Chinese Tian Shan: An early effect of the India-Asia collision. *Geology* **1994**, *22*, 487–490. [CrossRef]
10. Wang, Y.N.; Cai, K.D.; Sun, M.; Xiao, W.J.; Grave, J.D.; Wan, B.; Bao, Z.H. Tracking the multistage exhumation history of the western Chinese Tianshan by Apatite Fission Track (AFT) dating: Implication for the preservation of epithermal deposits in the ancient orogenic belt. *Ore Geol. Rev.* **2018**, *100*, 111–132. [CrossRef]
11. Nachtergaele, S.; De Pelsmaeker, E.; Glorie, E.; Zhimulev, F.; Jolivet, M.; Danisík, M.; Buslov, M.M.; De Grave, J. Mesozoic-Cenozoic tectonic evolution of the Talas-Fergana region of the Kyrgyz Tien Shan revealed by low-temperature basement and detrital thermochronology. *Geosci. Front.* **2018**, *9*, 1495–1514. [CrossRef]
12. Zhang, B.; Chen, W.; Liu, J.Q.; Yin, J.Y.; Sun, J.B. Thermochronological insights into the intracontinental orogeny of the Chinese western Tianshan orogen. *J. Asian Earth Sci.* **2020**, *194*, 103927. [CrossRef]
13. Zhu, W.B.; Shu, L.S.; Wan, J.L.; Sun, Y.; Wang, F.; Zhao, Z.Y. Fission-track evidence for the exhumation history of Bogda-Harlik Mountains, Xinjiang since the Cretaceous. *Acta Geol. Sin.* **2006**, *80*, 16–22, (In Chinese with English abstract).
14. Wang, X.W.; Wang, X.W.; Ma, Y.S. Differential exhumation history of Bogda Mountain, Xinjiang, Northwestern China since the Late Mesozoic. *Acta Geol. Sin.* **2007**, *11*, 1507–1517, (In Chinese with English abstract).
15. Wang, Z.X.; Li, T.; Zhang, J.; Liu, Y.Q.; Ma, Z.J. The uplift progresses of the Bogda Moutain and its significance. *Sci. China (Ser. D Geosci.)* **2008**, *38*, 316–326, (In Chinese with English abstract).
16. Tang, W.H.; Zhang, Z.C.; Li, J.F.; Li, K.; Luo, Z.W.; Chen, Y. Mesozoic and Cenozoic uplift and exhumation of the Bogda Mountain, NW China: Evidence from apatite fission track analysis. *Geosci. Front.* **2015**, *6*, 617–625. [CrossRef]
17. Zhang, X.; Nie, F.J.; Su, X.B.; Xia, F.; Li, M.G.; Yan, Z.B.; Zhang, C.Y.; Feng, Z.B. Relationships between Mesozoic-Cenozoic denudation in the Eastern Tian Shan and uranium mineralization in the Turpan-Hami basin, NW China: Constraints from apatite fission track study. *Ore Geol. Rev.* **2020**, *127*, 103820.
18. He, Z.Y.; Glorie, S.; Wang, F.J.; Zhu, W.B.; Fonseca, A.; Su, W.B.; Zhong, L.L.; Zhu, X.; De Grave, J. A re-evaluation of the Meso-Cenozoic thermo-tectonic evolution of Bogda Shan (Tian Shan, NW China) based on new basement and detrital apatite fission track thermochronology. *Int. Geol. Rev.* **2022**. [CrossRef]
19. He, Z.Y.; Wang, B.; Glorie, S.; Su, W.B.; Ni, X.H.; Jepson, G.; Liu, J.S.; Zhong, L.L.; Gillespie, J.; De Grave, J. Mesozoic building of the Eastern Tianshan and East Junggar (NW China) revealed by low-temperature thermochronology. *Gondwana Res.* **2022**, *103*, 37–53. [CrossRef]
20. Gillespie, J.; Glorie, S.; Jepson, G.; Zhang, Z.Y.; Xiao, W.J.; Danišík, M.; Collins, A.S. Differential exhumation and crustal tilting in the easternmost Tianshan (Xinjiang, China), revealed by low-temperature thermochronology. *Tectonics* **2017**, *36*, 2142–2158. [CrossRef]
21. Chen, Y.; Wang, G.C.; Kapp, P.; Shen, T.Y.; Zhang, P.; Zhu, C.Y.; Cao, K. Episodic exhumation and related tectonic controlling during Mesozoic in the Eastern Tian Shan, Xinjiang, northwestern China. *Tectonophysics* **2020**, *796*, 228647. [CrossRef]
22. Cunningham, D.; Owen, L.A.; Snee, L.; Li, J. Structural framework of a major intracontinental orogenic termination zone: The easternmost Tien Shan, China. *J. Geol. Soc.* **2003**, *160*, 575–590. [CrossRef]
23. Morin, J.; Jolivet, M.; Barrier, L.; Laborde, A.; Li, H.B.; Dauteuil, O. Planation surfaces of the Tian Shan Range (Central Asia): Insight on several 100 million years of topographic evolution. *J. Asian Earth Sci.* **2019**, *177*, 52–65. [CrossRef]
24. Jahn, B.; Wu, F.; Chen, B. Granitoids of the Central Asian Orogenic Belt and continental growth in the Phanerozoic. *Earth Environ. Sci. Trans. R. Soc. Edinb.* **2000**, *91*, 181–193.
25. Ji, H.J.; Tao, H.F.; Wang, Q.; Qiu, Z.; Ma, D.X.; Qiu, J.L.; Liao, P. Early to Middle Jurassic tectonic evolution of the Bogda Mountains, Northwest China: Evidence from sedimentology and detrital zircon geochronology. *J. Asian Earth Sci.* **2018**, *153*, 57–74. [CrossRef]
26. Li, J.Y. Late Neoproterozoic and Paleozoic tetonic framework and evolution of Eastern Xinjiang, NW China. *Geol. Rev.* **2004**, *50*, 304–322, (In Chinese with English abstract).

27. Wartes, M.A.; Carroll, A.R.; Greene, T.J.; Cheng, K.; Ting, H. Permian Lacustrine Deposits Of Northwest China. In Gierlowski-Kordesch, E., and Kelts, K., eds., Lake Basins through Space and Time. *Am. Assoc. Pet. Geol. Stud. Geol.* **2000**, *46*, 123–132.
28. Greene, T.J.; Carroll, A.R.; Wartes, M.; Graham, S.A.; Wooden, J.L. Integrated Provenance Analysis of a Complex Orogenic Terrane: Mesozoic Uplift of the Bogda Shan and Inception of the Turpan-Hami Basin, NW China. *J. Sediment. Res.* **2005**, *75*, 251–267. [CrossRef]
29. Chen, K.; Lin, W.; Wang, Q.C. The Bogeda Shan uplifting: Evidence from multiple phases of deformation. *J. Asian Earth Sci.* **2015**, *99*, 1–12. [CrossRef]
30. Yang, W.; Jolivet, M.; Dupont-Nivet, G.; Guo, Z.J.; Zhang, Z.C.; Wu, C.D. Source to sink relations between the Tian Shan and Junggar Basin (northwest China) from Late Palaeozoic to Quaternary: Evidence from detrital U-Pb zircon geochronology. *Basin Res.* **2012**, *25*, 219–240. [CrossRef]
31. Gu, L.X.; Yu, C.S.; Li, H.Y.; Xiao, X.J.; Yan, Z.F. Rb-Sr Isotope Age of the Shangdaheyan Intrusion in the Bogda Orogenic Belt and its Geological Implications. *Bull. Mineral. Petrol. Geochem.* **1999**, *19*, 19–21, (In Chinese with English abstract).
32. Zhang, X.B.; Chai, F.M.; Chen, C.; Quan, H.Y.; Gong, X.P. Geochronology, geochemistry and tectonic implications of Late Carboniferous Daheyan intrusions from the Bogda Mountains, eastern Tianshan. *Geol. Mag.* **2019**, *157*, 289–306. [CrossRef]
33. Hurford, A.J.; Green, P.F. The zeta-age calibration of fission-track dating. *Isot. Geosci.* **1983**, *1*, 285–317. [CrossRef]
34. Ketcham, R.A. Forward and inverse modeling of low-temperature thermochronometry data. *Rev. Mineral. Geochem.* **2005**, *58*, 275–314. [CrossRef]
35. Sobel, E.R.; Seward, D. Influence of etching conditions on apatite fission-track etch pit diameter. *Chem. Geol.* **2010**, *271*, 59–69. [CrossRef]
36. Hurford, A.J. Standardization of fission track dating calibration: Recommendation by the fission track working group of the I.U.G.S. Subcommission on Geochronology. *Chem. Geol.* **1990**, *80*, 171–178. [CrossRef]
37. Naeser, C.W.; Cebula, G.T. Recollection of Fish Canyon Tuff for fission-track standardization. *Nucl. Tracks Radiat. Meas.* **1985**, *10*, 393. [CrossRef]
38. Vermeesch, P. RadialPlotter: A Java application for fission track, luminescence and other radial plots. *Radiat. Meas.* **2009**, *44*, 409–410. Available online: http://www.ucl.ac.uk/~{}ucfbpve/radialplotter/ (accessed on 16 June 2021). [CrossRef]
39. Galbraith, R.F. On statistical estimation in fission track dating. *J. Int. Assoc. Math. Geol.* **1981**, *13*, 471–478. [CrossRef]
40. Donelick, R.A.; Ketcham, R.A.; Carlson, W.D. Variability of apatite fission-track annealing kinetics: II. Crystallographic orientation effects. *Am. Mineral.* **1999**, *84*, 1224–1234. [CrossRef]
41. Ketcham, R.A.; Carter, A.; Donelick, R.A.; Barbarand, J.; Hurford, A.J. Improved modeling of fission track annealing in apatite. *Am. Mineral.* **2007**, *92*, 789–798. [CrossRef]
42. Green, P.E.; Duddy, I.R.; Gleadow, A.I.W.; Tingate, P.R. Fission track annealing in apatite: Track length measurements and the form of the Arrhenius plot. *Nucl. Tracks* **1985**, *10*, 323–328. [CrossRef]
43. Vermeesch, P. How many grains are needed for a provenance study? *Earth Planet. Sci. Lett.* **2004**, *224*, 441–451. [CrossRef]
44. Ketcham, R.A.; Donelick, R.A.; Balestrieri, M.L.; Zattin, M. Reproducibility of apatite fission-track length data and thermal history reconstruction. *Earth Planet. Sci. Lett.* **2009**, *284*, 504–515. [CrossRef]
45. Barbarand, J.; Hurford, T.; Carter, A. Variation in apatite fission-track length measurement: Implications for thermal history modelling. *Chem. Geol.* **2003**, *198*, 77–106. [CrossRef]
46. Ketcham, R.A.; Donelick, R.A.; Carlson, W.D. Variability of apatite fission-track annealing kinetics: III. Extrapolation to geological time scales. *Am. Mineral.* **1999**, *84*, 1235–1255. [CrossRef]
47. Ketcham, R.A.; Donelick, R.A.; Donelick, M.B. AFTSolve: A program for multi-kinetic modeling of apatite fission-track data. *Am. Mineral.* **2003**, *88*, 929.
48. Wang, X.T. Stratigraphic Framework and Sedimentary Evolution of the Permian-Jurassic Strata in the Surrounding Area of the Bogda Mountains. Master's Thesis, China University of Petroleum (East China), Qingdao, China, 2017; pp. 1–119, (In Chinese with English Abstract).
49. Lu, M.A. Multistage Evolution of the Basin-and-Range Structure of the Eastern Section of the Tienshan Mountains. Ph.D. Thesis, Institute of Geology, China Earthquake Administration, Beijing, China, 2007; pp. 1–393, (In Chinese with English Abstract).
50. Guo, W. Intraplate Tectonics of Bogda Mountain in Xingjiang and Its Adjacent Plates. Ph.D. Thesis, Northwest University, Xi'an, China, 2008; pp. 1–163, (In Chinese with English Abstract).
51. Wu, Y.P. Structural deformation and Structural evolution characteristics in the northern of Bogda Mountains. Master's Thesis, Hefei University of Technology, Hefei, China, 2019; pp. 1–70, (In Chinese with English Abstract).
52. Liang, X.X.; Chen, S.; Chen, S.P.; Yuan, H.W.; Liang, Y.Y.; Song, X.G. Multi-stage deformation of Sangezhuang Uplift in the western margin of Bogda Mountain and its response to regional tectonic evolution. *Sci. Technol. Eng.* **2020**, *20*, 11455–11462, (In Chinese with English Abstract).
53. Gong, L.; Barry, P.K.; Zhang, Z.Y.; Xiao, B.; Wu, L.; Chen, H.Y. Exhumation and Preservation of Paleozoic Porphyry Cu Deposits: Insights from the Yandong Deposit, Southern Central Asian Orogenic Belt. *Econ. Geol.* **2021**, *116*, 607–628. [CrossRef]
54. Jepson, G.; Glorie, S.; Konopelko, D.; Mirkamalov, R.; Danišík, M.; Collins, A.S. The low-temperature thermo-tectonic evolution of the western Tian Shan, Uzbekistan. *Gondwana Res.* **2018**, *64*, 122–136. [CrossRef]

55. Glorie, S.; Otasevic, A.; Gillespie, J.; Jepson, G.; Danišík, M.; Zhimulev, F.I.; Gurevich, D.; Zhang, Z.; Song, D.; Xiao, W.J. Thermo-tectonic history of the Junggar Alatau within the Central Asian Orogenic Belt (SE Kazakhstan, NW China): Insights from integrated apatite U/Pb, fission track and (U-Th)/He thermochronology. *Geosci. Front.* **2019**, *10*, 2153–2166. [CrossRef]

56. De Grave, J.; Glorie, S.; Buslov, m.m.; Izmer, A.; Fournier-Carrie, A.; Batalev, V.Y.; Vanhaecke, F.; Elburg, M.; Van den haute, P. The thermo-tectonic history of the Song-Kul plateau, Kyrgyz Tien Shan: Constraints by apatite and titanite thermochronometry and zircon U/Pb dating. *Gondwana Res.* **2011**, *20*, 745–763. [CrossRef]

57. De Grave, J.; Glorie, S.; Buslov, M.M.; Stockli, D.F.; McWilliams, M.O.; Batalev, V.Y.; Van den haute, P. Thermo-tectonic history of the Issyk-Kul basement (Kyrgyz Northern Tien Shan, Central Asia). *Gondwana Res.* **2013**, *23*, 998–1020. [CrossRef]

58. Jepson, G.; Glorie, S.; Khudoley, A.K.; Malyshev, S.V.; Gillespie, J.; Glasmacher, U.A.; Carrapa, B.; Soloviev, A.V.; Collins, A.S. The Mesozoic exhumation history of the Karatau-Talas range, western Tian Shan, Kazakhstan-Kyrgyzstan. *Tectonophysics* **2021**, *814*, 228977. [CrossRef]

59. He, Z.Y.; Wang, B.; Su, W.B.; Glorie, S.; Ni, X.H.; Liu, J.S.; Cai, D.X.; Zhong, L.L.; De Grave, J. Meso-Cenozoic thermo-tectonic evolution of the Yili block within the Central Asian Orogenic Belt (NW China): Insights from apatite fission track thermochronology. *Tectonophysics* **2022**, *823*, 229194. [CrossRef]

60. Hendrix, M.S.; Graham, S.A.; Carroll, A.R.; Sobel, E.R.; Mcknight, C.L.; Schulein, B.J.; Wang, Z.X. Sedimentary record and climatic implications of recurrent deformation in the Tian Shan: Evidence from Mesozoic strata of the north Tarim, south Junggar, and Turpan basins, northwest China. *Geol. Soc. Am. Bull.* **1992**, *104*, 53–79. [CrossRef]

61. Dumitru, T.A.; Zhou, D.; Chang, E.Z.; Graham, S.A. Uplift, exhumation, and deformation in the Chinese Tian Shan. In: Hendrix, M.S., Davis, G.A. (Eds.), Paleozoic and Mesozoic tectonic evolution of central Asia: From continental assembly to intracontinental deformation. *Geol. Soc. Am. Mem.* **2001**, *194*, 71–99.

62. Jolivet, M.; Dominguez, S.; Charreau, J.; Chen, Y.; Li, Y.G.; Wang, Q.C. Mesozoic and Cenozoic tectonic history of the central Chinese Tian Shan: Reactivated tectonic structures and active deformation. *Tectonics* **2010**, *29*, 6019. [CrossRef]

63. Choulet, F.; Chen, Y.; Cogne, J.P.; Rabillard, A.; Wang, B.; Lin, W.; Faure, M.; Cluzel, D. First triassic palaeomagnetic constraints from Junggar (NW China) and their implications for the Mesozoic tectonics in central Asia. *J. Asian Earth Sci.* **2013**, *78*, 371–394. [CrossRef]

64. Wang, Y.; Sun, G.H.; Li, J.Y. U-Pb (SHRIMP) and 40 Ar/ 39 Ar geochronological constraints on the evolution of the Xingxingxia shear zone, NW China: A Triassic segment of the Altyn Tagh fault system. *Geol. Soc. Am. Bull.* **2010**, *122*, 487–505. [CrossRef]

65. Liu, B.; Chen, Z.L.; Yuan, F.; Zhang, Q.; Han, F.B.; Zhang, W.G.; Huo, H.L.; Li, J.L.; Zhao, T.Y.; Han, Q.; et al. Late Triassic dextral strike slip in the eastern segment of the shear zone on the northern margin of the Central Tianshan Mountains: Response to orogenic revival on the southwestern margin of the Central Asian orogenic belt. *Xinjiang Geol.* **2022**, *40*, 85–91. (In Chinese)

66. Glorie, S.; De Grave, J.; Buslov, M.M.; Elburg, M.A.; Stockli, D.F.; Gerdes, A.; Van den Haute, P. Multi-method chronometric constraints on the evolution of the Northern Kyrgyz Tien Shan granitoids (Central Asian Orogenic Belt): From emplacement to exhumation. *J. Asian Earth Sci.* **2010**, *38*, 131–146. [CrossRef]

67. Macaulay, E.A.; Sobel, E.R.; Mikolaichuk, A.; Kohn, B.; Stuart, F.M. Cenozoic deformation and exhumation history of the Central Kyrgyz Tien Shan. *Tectonics* **2014**, *33*, 135–165. [CrossRef]

68. Wang, G.; Zhang, M.; Zhang, X.; Liao, Q.; Wang, W.; Tian, J.; Xuan, Z.Y. Significant Paleozoic tectonic events in the northern part of the East Tianshan Mountains, Xinjiang and their implications for the evolution of CAOB: New evidence from 1:50000 geological survey of Banfanggou and Xiaoliugou sheets. *Geol. China* **2019**, *46*, 954–976, (In Chinese with English abstract).

69. XBGMR (Xinjiang Bureau of Geology and Mineral Resources). 1965; Volume 1, 200000, Geological map, Urumqi sheet (K-45-IV).

70. Zhang, K.J. Genesis of the Late Mesozoic Great Xing'an Range Large Igneous Province: A Mongol–Okhotsk slab window model. *Int. Geol. Rev.* **2014**, *56*, 1557–1583. [CrossRef]

71. Zhang, K.J.; Yan, L.L.; Ji, C. Switch of NE Asia from extension to contraction at the mid-Cretaceous: A tale of the Okhotsk oceanic plateau from initiation by the Perm Anomaly to extrusion in the Mongol–Okhotsk ocean? *Earth-Sci. Rev.* **2019**, *198*, 102941. [CrossRef]

72. Fang, Y.N.; Wu, C.D.; Wang, Y.Z.; Hou, K.J.; Guo, Z.J. Topographic evolution of the Tianshan Mountains and their relation to the Junggar and Turpan Basins, Central Asia, from the Permian to the Neogene. *Gondwana Res.* **2019**, *75*, 47–67. [CrossRef]

73. Guo, Z.J.; Zhang, Z.C.; Fang, S.H.; Fang, S.H.; Zhang, R. The Mesozoic and Cenozoic exhumation history of Tianshan and comparative studies to the Junggar and Altai Mountains. *Acta Geol. Sin.* **2006**, *80*, 1–15, (In Chinese with English abstract).

74. Zhang, Z.C.; Guo, Z.J.; Wu, C.D.; Fang, S.H. Thermal history of the Jurassic Strata in the Northern Tianshan and its geological significance, revealed by apatite fission track and vitrinite-reflectance analysis. *Acta Petrol. Sin.* **2007**, *23*, 1638–1695, (In Chinese with English abstract).

75. Zhu, W.B.; Wan, J.L.; Shu, L.S.; Zhang, Z.Y.; Su, J.B.; Sun, Y.; Guo, J.C.; Zhang, X.Y. Late Mesozoic Thermotectonic Evolution of the Jueluotage Range, Eastern Xinjiang, Northwest China: Evidence from Apatite Fission Track Data. *Acta Geol. Sin. (Engl. Ed.)* **2008**, *82*, 348–357.

76. Zhao, X.D.; Zhang, H.P.; Lü, H.H.; Lü, Y.Y.; Li, X.M.; Liu, K.; Zhang, J.W.; Xiong, J.G. Signatures of tectonic-climatic interaction during the Late Cenozoic orogenesis along the northern Chinese Tian Shan. *Basin Res.* **2021**, *33*, 291–311. [CrossRef]

77. Sun, J.M.; Zhu, R.X.; Bowler, J. Timing of the Tianshan Mountains uplift constrained by magnetostratigraphic analysis of molasse deposits. *Earth Planet. Sci. Lett.* **2004**, *219*, 239–253. [CrossRef]

78. Tang, Z.H.; Huang, B.C.; Dong, X.X.; Ji, J.L.; Ding, Z.L. Anisotropy of magnetic susceptibility of the Jingou River section: Implications for late Cenozoic uplift of the Tian Shan. *Geochem. Geophys. Geosystems* **2012**, *13*, Q03022.

79. Sun, J.M.; Zhang, Z.Q. Syntectonic growth strata and implications for late Cenozoic tectonic uplift in the northern Tian Shan, China. *Tectonophysics* **2009**, *463*, 60–68. [CrossRef]

80. Yin, A.; Nie, S.; Craig, P.; Harrison, T.M. Late Cenozoic tectonic evolution of the southern Chinese Tian Shan. *Tectonics* **1998**, *17*, 1–27. [CrossRef]

81. Wang, X.; Suppe, J.; Guan, S.W.; Hubert-Ferrari, A.; Gonzalez-Mieres, R.; Jia, C.Z. Cenozoic Structure and Tectonic Evolution of the Kuqa Fold Belt, Southern Tianshan, China. *Am. Assoc. Pet. Geol.* **2011**, *94*, 215–243.

82. Yu, S.; Chen, W.; Evans, N.J.; McInnes, B.I.A.; Yin, J.Y.; Sun, J.B.; Li, J.; Zhang, B. Cenozoic uplift, exhumation and deformation in the north Kuqa Depression, China as constrained by (U-Th)/He thermochronometry. *Tectonophysics* **2014**, *630*, 166–182. [CrossRef]

83. Guo, C.; Zhang, Z.Y.; Malusà, M.G.; Chew, D.; Xiang, D.F.; Wu, L.; Wang, N.; Xiao, W.J. Late Cenozoic topographic growth of the South Tianshan Mountain Range: Insights from detrital apatite fission-track ages, northern Tarim Basin margin, NW China. *J. Asian Earth Sci.* **2022**, *234*, 105277. [CrossRef]

84. Sun, Y.B.; Yan, Y.; Nie, J.S.; Li, G.J.; Shi, Z.G.; Qiang, X.K.; Chang, H.; An, Z.S. Source-to-sink fluctuations of Asian aeolian deposits since the late Oligocene. *Earth-Sci. Rev.* **2020**, *200*, 102963. [CrossRef]

85. Käßner, A.; Ratschbacher, L.; Jonckheere, R.; Enkelmann, E.; Khan, J.; Sonntag, B.L.; Gloaguen, R.; Gadoev, M.; Oimahmadov, I. Cenozoic intracontinental deformation and exhumation at the northwestern tip of the India-Asia collision-southwestern Tian Shan, Tajikistan, and Kyrgyzstan. *Tectonics* **2016**, *35*, 2171–2194. [CrossRef]

86. Xiang, D.F.; Zhang, Z.Y.; Xiao, W.J.; Zhu, W.B.; Zheng, D.W.; Li, G.W.; Zheng, B.H.; Song, D.F.; Han, C.M.; Pang, J.Z. Episodic Mesozoic-Cenozoic denudation of Chinese Tianshan: Evid-ence from detrital apatite fission track and zircon U-Pb data, southern Junggar Basin margin, NW China. *J. Asian Earth Sci.* **2018**, *175*, 199–212. [CrossRef]

87. Glorie, S.; De Grave, J. Exhuming the Mesozoic-Cenozoic Kyrgyz Tianshan and Siberian Altai-Sayan: A review based on low-temperature thermochronology. *Geosci. Front.* **2016**, *7*, 155–170. [CrossRef]

88. Jia, Y.Y.; Sun, J.M.; Lü, L.X. Late Cenozoic tectono-geomorphologic evolution of the northern Tian Shan mountain range: Insight from U-Pb ages of detrital zircon grains from the Upper Oligocene-Quaternary sediments of the southern Junggar basin. *J. Asian Earth Sci.* **2020**, *194*, 104286. [CrossRef]

89. Qin, X.; Chen, X.H.; Shao, Z.G.; Zhang, Y.P.; Wang, Y.C.; Li, B. Cenozoic multi-phase intracontinental deformation of the Tianshan Range (NW China): Constraints from detrital zircon provenance and syn-tectonic sedimentation of the Kuqa Depression. *J. Asian Earth Sci.* **2022**, *232*, 105183. [CrossRef]